Published in final edited form as:
Mol Genet Metab. 2009 June ; 97(2): 155–162. doi:10.1016/j.ymgme.2009.02.010.

The male sterility and histoincompatibility (*mshi*) mutation in mice is a natural variant of microtubule-associated protein 7 (*Mtap7*)

D. R. Magnan, **D. V. Spacek**, **N. Ye**, **Y.-C. Lu**, and **T. R. King***
Department of Biomolecular Sciences, Central Connecticut State University, 1615 Stanley Street, New Britain, CT 06053, USA

Abstract

Males homozygous for the mouse male sterility and histoincompatibility (*mshi*) mutation exhibit small testes and produce no sperm. In addition, *mshi* generates an "antigen-loss" histoincompatibility barrier, such that homozygous mutants reject skin grafts from wild-type co-isogenic BALB/cByJ donors. To facilitate the molecular characterization of the pleiotropic *mshi* mutation, we genetically mapped *mshi* into a 0.68 megabasepair region which contains fewer than 10 candidate genes. Complementation testing showed that one of these, *Mtap7*, is disrupted in *mshi* mice. Sequence analysis has revealed a 13 kilobasepair deletion in BALB/cByJ-*mshi*/J mice that begins in Intron 10–11 of *Mtap7*, and ends less than 2,000 base pairs downstream of the wild type gene. Analysis of the mutant cDNA predicts that $Mtap7^{mshi}$ encodes a 457 amino acid protein, the first 423 of which are identical to wild type, and the last 34 of which are due to aberrant mRNA splicing with two cryptic exons in the *Mtap7* to *P04Rik* intergenic region. This molecular assignment for the *mshi* mutation further supports an essential role for microtubule stabilization in spermatogenesis and indicates a new role in allograft transplantation.

Keywords

Spermatogenesis; E-MAP-115; Positional cloning; Complementation testing

1. Introduction

The mouse male sterility and histoincompatibility (*mshi*) mutation was identified by Don Bailey (The Jackson Laboratory, Bar Harbor, ME) in a large-scale screen for spontaneous histocompatibility mutants among a population of BALB/cByJ mice [1]. This mutation controls an "antigen-loss" histoincompatibility phenotype, such that homozygous (*mshi*/*mshi*) mutants reject skin grafts from wild type, coisogenic BALB/cByJ donors. In trying to establish an inbred line homozygous for *mshi*, it became immediately apparent that male homozygotes never bred, and exhibited small testes. Therefore, the BALB/cByJ-*mshi*/J strain has been maintained by mating homozygous females (identified by rejection of wild type BALB/cBy/J tail-skin grafts) with heterozygous (*mshi*/+) fertile males. Characterization of the *mshi* mutation, first described by Ward-Bailey et al. [2], has largely focused on these two pleiotropic aspects of the mutant phenotype, as summarized below.

*Corresponding Author: Thomas R. King, Address: Biomolecular Sciences/NC 204, Central Connecticut State University, 1615 Stanley Street, New Britain, CT 06053, Telephone: (860)-832-2654, FAX: (860)-832-3562, e-mail: kingt@ccsu.edu.

Males homozygous for the *mshi* mutation are sterile due to spermatogonial dysgenesis, identifiable by light microscopy at 3 weeks of age [2,3], and by external palpation of adults [4]. By 8 weeks, mutant testes (combined) weigh generally less than 0.1 g (0.08 ± 0.02) compared with heterozygotes and wild type mice, the testes of which are at least twice as massive (0.24 ± 0.02) [4]. Adult mutant testes contain tubules of small diameter, which are populated predominantly by Leydig and Sertoli cells, with only rare spermatogonia present. The tubules of adults are nearly devoid of active spermatogenesis. Time-course analysis shows that the migration to and subsequent proliferation of germ cells in the pre-pubescent mutant testis is normal [3,5]. However at 3.5 weeks (the onset of puberty), spermatogonia gradually disappear, and by adulthood germ cells are mostly absent, except for rare spermatogonia, and some spermatocytes in early meiotic stages. Ward-Bailey et al. [2] suggest that the suddenly reduced numbers of spermatogonia by 5 weeks of age may be due to a failure to replace the differentiating spermatogenic population after initiation of the first wave of spermatogenesis, but Lanza [3] suggests that spermatogonia are lost due to apoptosis (detected by the terminal deoxynucleotidyltransferase-mediated dUTP nick-end labeling, or TUNEL, method). In either case, the *mshi* mutation appears to provide a valuable animal model for studying the biology of cellular differentiation in general and spermatogenesis in particular (see [6], for example).

The *mshi* mutation also appears to cause a typical antigen-loss histoincompatibility phenotype, in that homozygous mutants reject skin grafts from wild-type BALB/cByJ donors (with a mean rejection time of just under 9 weeks post surgery [4]). However, *mshi* may not fit the standard "two-part" model for minor histocompatibility (*H*) locus structure [7]. While T-cell-depletion studies have shown a critical role for helper T cells in this allograft reaction, no role for cytotoxic T cells (CTL) can be demonstrated [8], and multiple attempts to isolate specifically reactive CTL have all failed (our unpublished data). Thus, *mshi* may identify a different type of minor *H* locus: one that includes a "T-helper cell-defined" or HD component, but which lacks a "CTL-defined" or CD component [9]. Furthermore, our explicit attempt to meiotically separate *H-mshi* into two components has failed, in spite of more than 400 backcross progeny screened [10]. This result, combined with the historical association of both the male-sterility and histoincompatibility phenotypes of the *mshi* mutation (in spite of selection for only the male-sterility phenotype) suggests that *mshi*-mediated allograft rejection could result from the mutation of only a single locus (rather than the usual two). Finally, we have shown that the wild-type H-*mshi* antigen(s) are conserved among all laboratory strains tested (by tail skin graft-exchange assay), including the wild-derived CAST/Ei and SPRET/Ei inbred strains [8].

In summary, previous work suggests that *mshi* may exemplify a new type of minor *H* locus that may have resulted from the mutation of a single, highly-conserved gene, and mediates an unusual, CTL-independent rejection mechanism. It seems also to control a genetic block in spermatogenesis such that germ cells, which mostly disappear at puberty, appear never to progress beyond mid-meiotic stages.

To facilitate the assignment of the *mshi* mutation to a particular gene (or genes), we have produced a genetic map for proximal mouse Chromosome (Chr) 10 that is based upon 402 meiotic events from a multi-point testcross segregating for *mshi* [4,10]. Archived DNA samples from these 402 backcross mice comprise a "panel" that can be used to genetically map any locus which is dimorphic between the two parental strains, C57BL/6J and BALB/cByJ-*mshi*/J. This mapping panel provides better than 0.2 centiMorgan (cM) resolution, which may correspond to about 500 kilobasepairs (Kb) of DNA between crossovers. Our previous analysis of this panel had placed both features controlled by *mshi* (male sterility and histoincompatibility) within a 1.7 cM interval between markers *D10Mit168* and *D10Mit213* [10], a region known to contain 1.6 megabasepairs (Mb) of DNA and fewer than 15 known genes [11]. Here, we describe the use of this high-resolution genetic map to finally determine the molecular nature of the genetic disruption that resulted in the spontaneous *mshi* mutation.

2. Materials and methods

2.1 Mice

All mice used in this study were obtained from The Jackson Laboratory (Bar Harbor, ME, USA), including mice from the standard inbred strains BALB/cByJ and C57BL/6J, the co-isogenic BALB/cByJ-*mshi*/J strain, and mice of a mixed genetic background that carried the *Mtap7*$^{Gt(ROSABetageo)1Sor}$ knock-out mutation (designated here as *Mtap7*$^{k.o.}$). Creation of the *Mtap7*$^{k.o.}$ mutation is described by Komada et al. [12], who used a retroviral gene-trap vector containing a *βgal*/*neo* fusion gene to infect embryonic stem cells. The *βgal*/*neo* cassette was flanked by a splice acceptor site and the bovine growth hormone polyadenylation signal [13], and its insertion within the 81.7 Kbp Intron 1-2 resulted in an in-frame fusion after alanine 23, creating a null allele. In our laboratory, *Mtap7*$^{k.o.}$ carriers have been backcrossed to C57BL/6J (to the N7 generation at the time this manuscript was submitted).

2.2 DNA isolation and analysis

Production of the large (C57BL/6J × BALB/cByJ-*mshi*/J)F_1 × BALB/cByJ-*mshi*/J backcross panel, and the isolation and initial characterization of those 402 genomic DNA samples, has been described previously [4,10]. Genomic DNA templates for genotyping individual mice from other crosses were isolated from tail tip biopsies taken from two-week old animals, using Nucleospin kits from BD Biosciences (Palo Alto, CA, USA), as directed.

Primers for *D7Mit#* microsatellite markers were obtained from the Research Genetics division of Clontech (Huntsville, AL, USA). To distinguish *Mtap7*$^{k.o.}$ carriers and wild type mice, genomic DNA templates were analyzed by the polymerase chain reaction (PCR), using forward and reverse primers from within the *neo* insertion as described by Tybulewicz et al. [14].

The polymerase chain reaction was performed in 13 μL reactions that contained 6 μM of each primer, and 50 ng/μL of template DNA. PCR reaction products were electrophoresed through 3.5% NuSieve agarose gels (Cambrex Bio Science, Rockland, ME, USA), stained with ethidium bromide (0.5 μg/mL), and photographed under ultraviolet light.

For DNA sequence analysis, about 1.5 μg of individual PCR amplimers were purified and concentrated into a 30 μl volume using QIAquick PCR Purification kits (Qiagen, Valencia, CA, USA). Amplimers were shipped to SeqWright (Houston, TX, USA) for primer-extension sequencing.

2.3 New DNA markers

The C57BL/6J vs. BALB/cByJ-derived alleles of *D10Csu1* (an alias for *Il20ra*) were distinguished on the basis of a single-nucleotide polymorphism in Exon 4 that destroys a *Bsl*I target site in the BALB/cByJ strain (see Table S1). Therefore, C57BL/6J-derived amplimers (442 bp) can be cut into 258, 121 and 63 bp fragments upon digestion with *Bsl*I; while the 438 bp BALB/c-derived amplimer yields 258, and 180 bp fragments only.

D10Csu2 (an alias for *P04Rik*) and *D10Csu3* (an alias for *Bclaf1*) are described in detail in Table S1. The C57BL/6J vs. BALB/cByJ-derived alleles of *D10Csu2* were distinguished on the basis of a single-nucleotide polymorphism in the 5′ untranslated region of the gene. The C57BL/6J vs. BALB/cByJ-derived alleles of *D10Csu3* were distinguished on the basis of a single-nucleotide polymorphism in Exon 5 that destroys a *Bst*F5I target site in the BALB/c strain. Therefore, C57BL/6-derived amplimers at *D10Csu3* (578 bp) can be cut into 282, 184 and 112 bp fragments upon digestion with *Bst*F5I; while the 576 bp BALB/cByJ-derived amplimer yields 466, and 110 bp fragments only.

2.4 RNA isolation and cDNA analysis

For cDNA analysis, total RNA was isolated from the testes of 10-week old males using the Nucleospin® RNA L kit by Macherey-Nagel (Easton, PA, USA). cDNA was generated and amplified using the SMART™ RACE cDNA Amplification Kit (Clontech Laboratories). For 3′ cDNA analysis, we used a gene-specific primer, *exon10F* 5′ ACATCCGGCCTGTCAAGAGAGAAGT 3′, taken from exon 10 of the *Mtap7* gene [11]. RACE products of interest were gel-purified using the Nucleotrap® Gel Extraction Kit (Clontech Laboratories), and isolated sequences were cloned directly into the pCR®4-TOPO® plasmid vector (Invitrogen Corp.; Carlsbad, CA, USA). Recombinant plasmids were transformed into One Shot® TOP10 *E.coli* (Invitrogen Corp.) from which 5 ug of plasmid DNA was purified and shipped to SeqWright (Houston, TX, USA) for primer-extension sequencing.

2.5 Histology and immunofluorescence staining

Testes to be examined by light microscopy were fixed in 10% formalin, embedded in paraffin, thin-sectioned at 5 μm, and stained with hematoxylin and eosin. For immunofluorescence staining, testes were fixed and sectioned as above. After removal of paraffin with xylene and rehydration, sections were blocked in PBS with 1% BSA for 30 minutes at 37° C, then incubated with rabbit anti-β-tubulin antibody (1:50 dilution; Cell Signaling Technology, Beverly, MA, USA) for 1 hour at 37°C followed by incubation with goat anti-rabbit Alexa 568 (1:1000 in PBS/BSA; Molecular Probes, Eugene, OR, USA) for 1 hour at room temperature. Nuclei were visualized by incubating sections with Hoechst stain (1:10,000 in PBS/BSA; Sigma-Aldrich, St. Louis, MO, USA) for 10 minutes at room temperature after the incubation with secondary antibodies. Fluorescent images were captured and processed using a SPOT camera (Diagnostic Instruments, Sterling Heights, MI, USA) attached to an inverted Nikon (Melville, NY, USA) microscope, and the images processed with Adobe Photoshop software (Adobe Systems, San Jose, CA, USA).

2.6 Tubule measurements

Four tubules from one testicular cross section of each mouse were selected at random, and measured to the nearest 5 um using the 10 × objective of a light microscope fitted with a micrometer. The diameter measured was that perpendicular to the longer axis of the tubule.

3. Results

3.1 Refinement of the genetic map

One of the genes known to lie in the *mshi*-critical interval between *D10Mit168* and *D10Mit213* is interleukin-20 receptor alpha (*Il20ra*). *Il20ra* encodes a transmembrane cell-surface protein [15], and is known to be expressed in both skin and testes [16], making it an apparent candidate for the gene that is disrupted in the *mshi* mutation. We found that *Il20ra* mRNA is highly expressed in both normal and *mshi*/*mshi* mutant skin, as well as in wild type testes, but found only a low level of expression in mutant testes [17]. To test *Il20ra* for a *mshi*-specific mutation, we sequenced the promoter, coding regions, and 3′ untranslated regions of the gene in wild type C57BL/6J, wild type BALB/cByJ, and BALB/cByJ-*mshi*/J mutant mice. While no *mshi*-specific changes were found, we did find several differences between C57BL/6J and BALB/cByJ in non-coding regions and one in Exon 4. The single nucleotide dimorphism in Exon 4 (designated *D10Csu1*, see Table S1) destroys a *Bsl*I restriction site in BALB/cByJ that is present in C57BL/6J. This C57BL/6J and BALB/cByJ dimorphism was used to type *Il20ra* alleles in mice from the 402-member mapping panel which were recombinant between *D10Mit16* and *D10Mit2*. This analysis identified five crossovers between *Il20ra* and *mshi* and one crossover between *mshi* and *D10Mit213*. This interval, which

measures 680 Kb and which must contain the *mshi* mutation, includes only seven known genes (see Fig. 1).

Sequence analysis of coding regions for two of these remaining gene candidates, *4933406P04Rik* (*Mus musculus* adult male testis cDNA, abbreviated *P04Rik* here) and *Bclaf1* (BCL2-associated transcription factor 1) [18], also failed to identify any *mshi*-specific alterations, but did reveal single-base dimorphisms between C57BL/6J and BALB/cByJ that provided easily-scored aliases *D10Csu2* (for *P04Rik*) and *D10Csu3* (for *Bclaf1*) (see Table S1). However, since no recombinants in the 402-member panel were found to separate *mshi* from these markers, further map refinement on this flank was not possible.

3.2 Complementation testing between *Mtap7$^{k.o.}$* and *mshi*

To evaluate *Mtap7* as a potential candidate, we obtained mice that carry an engineered null allele of the gene (*Mtap7$^{Gt(ROSABetageo)1Sor}$*), here designated *Mtap7$^{k.o.}$*. This loss-of-function mutation was produced by Komada and coworkers [12] by the insertion of a *βgeo* cassette [13] downstream of the first exon of *Mtap7*, and results in expression of a fusion protein that includes only the first 21 amino acids of the Mtap7 protein. As with *mshi* homozygotes, males (but not females) homozygous for *Mtap7$^{k.o.}$* are sterile. To test this recessive mutation for complementation with *mshi*, we crossed *mshi/mshi* fertile females with heterozygous, fertile *Mtap7$^{k.o./}$*+ males. These testcrosses produced 9 females and 21 males, which were typed for *βgeo* to distinguish *Mtap7$^{k.o.}$* carriers and *Mtap7^{+}* controls.

When they had reached 8 weeks of age, all of these males were caged singly with fertile C57BL/6J females for 3 weeks. All males were equally able to copulate (as judged by the presence of vaginal plugs, data not shown), but while 6 of 6 control males produced pregnancies, none of 15 *Mtap7$^{k.o.}$* carrier males did. At 90 days of age, *Mtap7$^{k.o.}$* carrier males and control siblings were euthanized. Testes from individual males were dissected away from the epididymis and adhering fat, were weighed together to the nearest 0.01 g, and were fixed in formalin. Testes from *Mtap7$^{k.o.}$* carrier males were less than one-third of the size of their control littermates (see Fig. 2), with an average mass of 0.07 ± 0.01 g (n = 15) compared to 0.25 ± 0.02 g (n = 6) for controls, although there was no significant difference in body weights (data not shown). These results were not different from those obtained from control, age-matched *mshi*/*mshi* × *mshi*/+ and *Mtap7$^{k.o.}$*/*Mtap7$^{k.o}$*. × *Mtap7$^{k.o.}$*/+ testcrosses (Fig. 2B). The failure of the *Mtap7$^{k.o.}$* null allele to complement the *mshi* defect in compound heterozygotes suggests that the *mshi* mutation is (or at least includes) a defect in the *Mtap7* gene.

The histology of the testes from these 15, 90-day-old *Mtap7$^{k.o.}$* carrier males (and 4 controls) was examined in sections by light microscopy (see Fig. 3). Most strikingly, the diameter of the seminiferous tubules in the testes of *Mtap7$^{k.o.}$* carrier males (Fig. 3C) was significantly shorter than in controls (Fig 3A). The lumen of the tubules in *Mtap7$^{k.o.}$* carriers were absent, and tubules consisted mostly of Sertoli cells with occasional spermatogonia. Essentially the same contrast was seen between the testes from 3 heterozygous (wildtype) and 4 homozygous (mutant) males from control *mshi*/*mshi* × *mshi*/+ testcrosses (Fig. 3B, E); and between the testes from 5 heterozygous (wildtype) and 6 homozygous (mutant) males from control *Mtap7$^{k.o.}$*/*Mtap7$^{k.o}$*. × *Mtap7$^{k.o.}$*/+ testcrosses (Fig 3D, E).

In characterizing their *Mtap7$^{k.o.}$* null allele, Komada et al. [12] used immunofluorescence staining with an antibody against β-tubulin to implicate abnormal microtubule morphology as the primary defect that leads to germ cell depletion and tubule dysgenesis in *Mtap7$^{k.o.}$* homozygotes. To determine if the *mshi* mutation might similarly disrupt microtubule organization, we also stained for tubulin in our 90-day-old *mshi/mshi*, *mshi/Mtap7$^{k.o.}$*, and *Mtap7$^{k.o.}$*/*Mtap7$^{k.o.}$* testis cross sections. Control *mshi*/+ males showed spoke-like concentrations of tubulin that extended from the nucleus of the Sertoli cells toward the lumen

(Fig. 4A). In all three mutant tubules (*mshi/mshi*, *mshi/Mtap7*$^{k.o.}$, and *Mtap7*$^{k.o.}$/*Mtap7*$^{k.o.}$), tubulin staining showed diffuse expression of microtubules, but with little evidence for organization into bundles (Fig. 4B–D). So, *mshi*-generated sterility seems, in these ways, phenotypically similar to that described by Komada et al. [12] for the *Mtap7*$^{k.o.}$ null allele.

By contrast, while all mutant genotypes (*mshi/mshi*, *mshi/Mtap7*$^{k.o.}$, and *Mtap7*$^{k.o.}$/*Mtap7*$^{k.o.}$) showed some degree of extracellular vacuolization within the tubules (Fig. 3B,C), this characteristic was markedly more extensive in the tubules of the 9-week-old *Mtap7*$^{k.o.}$/*Mtap7*$^{k.o.}$ males in our study (Fig. 3D), suggesting that the degeneration of the tubule was more advanced in males with this genotype.

3.3 Sequence analysis of the *mshi* mutation

We examined the structure of the *Mtap7* gene carried by the C57BL/6J, BALB/cByJ, and BALB/cByJ-*mshi*/J strains by sequencing all known exons in these genomic DNAs, and by determining the 3′ ends of these *Mtap7* transcripts using the rapid amplification of cDNA ends (RACE) method [19]. The *Mtap7* gene in the BALB/cByJ-*mshi*/J strain showed no differences compared with BALB/cByJ in any of the first 10 exons (or the 10–100 bases of flanking intron sequences also sequenced). This analysis did reveal five natural dimorphisms (one each in Exon 4 and 9; three more in Exon 10) carried by these BALB/cByJ strains compared with the standard C57BL/6J strain (see Fig. S1), but all of these third-position variants were silent. By contrast, the *Mtap7* gene carried by the BALB/cByJ-*mshi*/J strain was characterized by a large, 13,080 bp deletion beginning at nucleotide 1,616 in Intron 10–11, and extending to nucleotide 1,959 of the 3′ downstream sequence beyond Exon 18 (which we define for the first time in wild-type testes mRNA, as shown in Fig. S1). Primers that flank the deletion were used in a standard polymerase chain reaction to determine the exact structure of these breakpoints in the mutant, and revealed a small insertion of the tetranucleotide, 5′ GCTC 3′ (see Fig. S2). 3′RACE indicated that in the mutant *mshi* transcript, Exon 10 is spliced to a cryptic exon, designated Exon 11M, which begins 4,213 bp downstream of the deletion breakpoint. Exon 11M (168 nucleotides) is spliced to another cryptic exon, designated Exon 12M (192 nucleotides) that is located 830 bp downstream of Exon 11M (Fig. S3). The resulting abnormal 1,724 nucleotide transcript is predicted to direct the translation of a 457 amino acid mutant protein (see Fig. S3).

4. Discussion

4.1 A molecular assignment for *mshi*-generated male sterility

Non-complementation between the *mshi* and *Mtap7*$^{k.o.}$ alleles shows that a defect in *Mtap7* alone is responsible for the male-sterility phenotype controlled by the spontaneous mouse *mshi* mutation. This result emphasizes a key role for microtubules in spermatogenesis (as described in detail by Komada et al. [12]). Mtap7 has been implicated in stabilizing and reorganizing microtubules during epithelial cell polarization [20] and its high level of expression has been shown in germ, Sertoli, and Leydig cells of the testis [12,20]. Whereas the mutant phenotypes displayed by *mshi* and *Mtap7*$^{k.o.}$ homozygotes clearly show a critical requirement for Mtap7 protein for normal germ and Sertoli cell function, an overt Leydig cell defect has not been described [2,12], and testosterone levels in mutants are in the normal range [2,5]. *Mtap7* is also known to be highly expressed in the intestines, kidney, and epidermis [12,20,21], but no morphological or histological alteration in these tissues has been noted for either mutant genotype (*Mtap7*$^{k.o.}$/*Mtap7*$^{k.o.}$ or *mshi/mshi*). Further study will be needed to clarify the functional role of *Mtap7* in these other epithelial tissues. In any case, we recommend that the *mshi* mutation be renamed *Mtap7*^{mshi}.

Spontaneous or inherited defects in the human orthologue of *Mtap7*, *MAP7*, are likely to cause male sterility in humans as well. Some 10 to 20% of infertile men display azoospermia [22],

and defective spermatogenesis is the basis of infertility in some 60% of patients with azoospermia [23]. One study suggests that about half of all cases of male infertility due to impaired spermatogenesis have a familial component [24]. However, genetic sterilities in man are inherently difficult to study [25] and none have yet been mapped to the orthologous region on human Chr 6q23 [26]. Perhaps direct screening of candidate genes like *MAP7* among infertile males with azoospermia will be useful in detecting mutations that can cause impaired spermatogenesis in man (see below).

Our analysis has also defined Exon 18 of the *Mtap7* transcript at least in the wild type testis, as well as a handful of silent single-nucleotide polymorphisms (vs. the C57BL/6 strain standard) that are carried in the BALB/cByJ inbred strain. The 3′ end of the mutant *Mtap7*^{mshi} transcript is shown here to include two exonic portions that follow the standard Exon 10, here designated as Exons 11M and 12M, that are encoded just downstream of the standard *Mtap7* gene sequence. Based on this, and our observation of apparently slower progress of tubule dysgenesis in *Mtap7*^{mshi}/*Mtap7*^{mshi} and *Mtap7*^{mshi}/*Mtap7*$^{k.o.}$ mice compared to *Mtap7*$^{k.o.}$/*Mtap7*$^{k.o.}$ mice at 90 days (see Fig. 3B–D), we predict that the *Mtap7*^{mshi} allele is expressed as a truncated protein product, which may retain some residual function which can (in *mshi*/*mshi* or *mshi*/*Mtap7*$^{k.o.}$ mice) somewhat retard the progression of the devastating germ- and Sertoli-cell defects that have been described in detail by Komada et al. [12] for *Mtap7*$^{k.o.}$ null-allele homozygotes. (Alternatively, this phenotypic distinction could merely be due to genetic-background differences among the three genotypes compared in Fig. 3.) Future work should focus on a tissue-by-tissue analysis of gene expression pattern at the mRNA and protein levels in both mutant and wild type mice.

4.2 Histocompatibilty aspects of *mshi*: A one vs. two-gene model

The molecular defect we describe in the BALB/cByJ-*mshi*/J mouse's *Mtap7* gene seems, based on its phenotypic similarity with the *Mtap7*$^{k.o.}$ mutant, entirely responsible for *mshi*-generated sterility. However, this mutation may or may not be the sole defect responsible for the histoincompatibility aspect of the *mshi*-mediated phenotype. Typically, *H*-variants are found to be the result of two mutational events in linked antigen-encoding loci, one that encodes a "T-helper cell-defined" or HD component, and a second that encodes a "CTL-defined" or CD component [7,9,27]. If this model applied to H-*mshi* locus structure, then a second mutation linked to the *Mtap7*^{mshi} deletion might remain to be discovered. However, this and previous studies suggest that *H-mshi* may not be a good fit for the standard two-gene model. Critically, no role for cytotoxic T cells (CTL) has been demonstrated for *mshi*-mediated allograft rejection [8], and both long-term backcrossing and high-resolution meiotic mapping have failed to separate the male sterility and histoincompatibility phenotypes generated by *mshi* [10]. Here we have extended this result by typing *Il20ra* among a subset of 135 males from the 402 member mapping panel, males which were typed both for testis morphology and histocompatibility by tail skin grafting. Analysis of these males showed that both the male sterility and histoincompatibility phenotypes co-localize in the *Il20ra* to *D10Mit213* interval, and remained linked even among four of these fully-typed males which carried a crossover between *Il20ra* and *D10Mit213*. So, if *H-mshi* really is comprised of two genes, only one of which is *Mtap7*, then any hypothetical second gene would be expected to lie less than about 680/4 or 170 Kb from *Mtap7*.

A single-gene model for *H-mshi* locus structure might explain both our inability to genetically dissect the *H-mshi* locus and our failure to find any evidence for a CD component. We propose that *Mtap7* likely encodes the HD component which has clearly been demonstrated for *H-mshi*-mediated allograft rejection [8]. Instead of a CD component, we propose that *Mtap7* also generates an "antibody-defined" (or AD) effector component of the allograft reaction. Genetic control of AD effector function may be direct or indirect, but in either case currently remains

undefined. Support for this proposal may be given by the *Mtap7*$^{k.o.}$ single-site, loss-of-function allele, which, under a one-gene model, is predicted to produce an antigen-loss histogenic phenotype similar to that of *H-mshi*. Testing this prediction, however, will require that the *Mtap7*$^{k.o.}$ allele first be established on a fully-inbred genetic background (in progress). A failure of *Mtap7*$^{k.o.}$ to mediate an alloantigenic rejection reaction would suggest instead that *H-mshi* results from a more complex mutation than we have currently defined with the *Mtap7*^{mshi} deletion.

A complete functional analysis of *H-mshi*, including a molecular immunogenetic identification of the HD and proposed AD components, is needed to finally distinguish between these one and two-gene models. Interestingly, definition of these immunological components may facilitate screening in humans for examples of male sterility that are caused by *MAP7* defects. For example, we envision an antibody-based skin test where even unaffected females homozygous for such mutations might be identified.

Supplementary Material

Refer to Web version on PubMed Central for supplementary material.

Acknowledgments

The authors wish to thank all the students who participated in this analysis, especially Endonesia Octave, Emilio Marin, Maryann Abogunde, Richard Haughton, Bizu Irving, Theresa Johnson, Kate Strathearn, and Romina Badal. We also thank Rachel Maloney and Mary Mantzaris for excellent animal care, and Drs. James Mulrooney and Kristi Lamonica for antibodies and guidance with immunofluorescence microscopy. This work was supported by research grants from Connecticut State University, the Connecticut Business and Industry Association (CBIA), and AREA Grant HD055666.

References

1. Bailey DW. Genetics of histocompatibility in mice I: New loci and congenic strains. Immunogenetics 1975;2:249.
2. Ward-Bailey PF, Johnson KR, Handel MA, Harris BS, Davisson MT. Male sterility and histoincompatibility (*mshi*): A new mutation on mouse Chromosome 10. Mammalian Genome 1996;7:793–797. [PubMed: 8875885]
3. Lanza, JR. MA dissertation. New Britain, CT: Central Connecticut State University; 2004. Abnormal apoptosis in sterile *mshi/mshi* mutant mice.
4. Turner JP, Carpentino JE, Cantwell AM, Hildebrandt AL, Myrie KA, King TR. Molecular genetics mapping of the mouse male sterility and histoincompatibility (*mshi*) mutation on proximal Chromosome 10. Genomics 1997;39:1–7. [PubMed: 9027480]
5. Myrie, KA. MA dissertation. New Britain, CT: Central Connecticut State University; 1997. Investigation odf the basis of male sterility in the *mshi*/*mshi mutant mouse*.
6. Clemente EJ, Furlong RA, Loveland KL, Affara NA. Gene expression study in the juvenile mouse testis: Identification of stage specific molecular pathways during spermatogenesis. Mammalian Genome 2006;17:956–975. [PubMed: 16964443]
7. Roopenian, DC. Lessons from *H3*, a model autosomal mouse minor histocompatibility locus. In: Roopenian, DR.; Simpson, E., editors. Minor histocompatibility antigens: From the laboratory to the clinic. Landes Bioscience; Georgetown, TX: 2000. p. 1-14.
8. Hildebrandt AL, Cantwell AM, Rule MR, King TR. The H-mshi antigen is conserved among standard BALB/cBy, C57BL/6J, and wild-derived CAST/Ei and SPRET/Ei inbred strains of mice. Immunogenetics 1999;49:666–672. [PubMed: 10369925]
9. Roopenian DC. What are minor histocompatibility loci? A new look at an old question. Immunology Today 1992;13:7–10. [PubMed: 1531413]

10. Rule MC, Mutcherson RJ II, Foss AD, Nguyen TK-X, Myrie KA, King TR. Mouse male sterility and histoincompatibility (*mshi*) maps between the *D10Mit51/168/212* cluster and D10Mit213. Mamm Genome 1999;10:447–450. [PubMed: 10337616]
11. Ensembl Mouse, Mouse Genome Sequencing Consortium: The European Bioinformaticics Institute (EBI) and the Welcome Trust Sanger Instituite (WTSI), Release 52, World Wide Web URL: < http://www.ensembl.org/Mus_musculus/> 2009.
12. Komada M, McLean DJ, Griswald MD, Russell LD, Soriano P. E-MAP-115, encoding a microtubule-associated protein, is a retinoic acid-inducible gene required for spermatogenesis. Genes & Development 2000;14:1332–1342. [PubMed: 10837026]
13. Friedrich G, Soriano P. Promoter traps in embryonic stem cells: A genetic screen to identify and mutate developmental genes in mice. Genes & Dev 1991;5:1513–1523. [PubMed: 1653172]
14. Tybulewicz VL, Crawford CE, Jackson PK, Bronson RT, Mulligan RC. Neonatal lethality and lymphopenia in mice with a homozygous disruption of the c-*abl* protooncogene. Cell 1991;65:1153–1163. [PubMed: 2065352]
15. Blumberg H, Conklin D, Xu W, Grossmann A, Brender T, Carollo S, Eagan M, Foster D, Haldeman BA, Hammond A, et al. Interleukin 20: Discovery, receptor identification, and role in epidermal function. Cell 2001;104:9–19. [PubMed: 11163236]
16. Parrish-Novak J, Xu W, Brender T, Yoa L, Jones C, West J, Brandt C, Jelinek L, Madden K, McKernan PA, et al. Interleukins 19, 20, and 24 signal through two distinct receptor complexes. J Biol Chem 2002;277:47517–47523. [PubMed: 12351624]
17. Lu, Y-C. MA dissertation. New Britain: CT Central Connecticut State University; 2004. Interleukin 20 receptor α is not the gene disrupted by the male sterility and histoincompatibility (*mshi*) mutation in mice.
18. Kawai J, Shinagawa A, Shibata K, Yoshino M, Itoh M, Ishii Y, Arakawa T, Hara A, Fukunishi Y, Konno H, et al. Functional annotation of a full-length mouse cDNA collection. Nature 2001;409:685–690. [PubMed: 11217851]
19. Zhu YY, Machleder EM, Chenchik A, Li R, Siebert PM. Reverse transcriptase template switching: A SMART approach for full-length cDNA library construction. Biotechniques 2001;30:892–897. [PubMed: 11314272]
20. Fabre-Jonca N, Allaman JM, Radlgruber G, Meda P, Kiss JZ, French LE, Masson D. The distribution of murine 115-kDa epithelial microtubule-associated protein (E-MAP-115) during embryogenesis and in adult organs suggests a role in epithelial polarization and differentiation. Differentiation 1998;63:169–180. [PubMed: 9745708]
21. Fabre-Jonca N, Viard I, French LE, Masson D. Up regulation and redistribution of E-MAP-115 (epithelial microtubule-associated protein of 115 kDa) in terminally differentiating keratinocytes is coincident with the formation of intercellular contacts. J Invest Dermatol 1999;112:216–225. [PubMed: 9989799]
22. Stanwell-Smith RE, Hendry WF. The prognosis of male infertility: A survey of 1025 men referred to a fertility clinic. Br J Urology 1984;56:422–428.
23. Matsumiya K, Namiki M, Takahara S, Kondoh N, Takada S, Kiyohara H, Okuyama A. Clinical study of azoospermia. Int J of Andrology 1994;17:140–142.
24. Gianotten J, Lombardi MP, Zwinderman AH, Lilford RJ, van der Veen F. Idiopathic impaired spermatogensis: Genetic epidemiology is unlikely to provide a short cut to better understanding. Human Reproduction Update 2004;10:533–539. [PubMed: 15465836]
25. Gianotten J, Westerveld GH, Leschot NJ, Tanck MWT, Lilford RJ, Lombardi MP, van der Veen F. Familial clustering of impaired spermatogensis: No evidence for a common genetic inheritance pattern. Human Reprod 2004;19:71–76.
26. Online Mendelian Inheritance in Man (OMIM), McKusick-Nathans Institute of Genetic Medicine, Johns Hopkins University (Baltimore, MD) and National Center for Biotechnology Information, National Library of Medicine (Bethesda, MD), World Wide Web URL:< http://www.ncbi.nlm.nih.gov/omim/> 2009.
27. King TR, Christianson GJ, Mitchell MJ, Bishop CE, Scott D, Ehrmann I, Simpson E, Eicher EM, Roopenian DC. Deletion mapping by immunoselection against the H-Y histocompatibility antigen

further resolves the *Sxr*^{a} region of the mouse Y chromosome and reveals complexity of the *Hya* locus. Genomics 1994;24:159–168. [PubMed: 7896271]

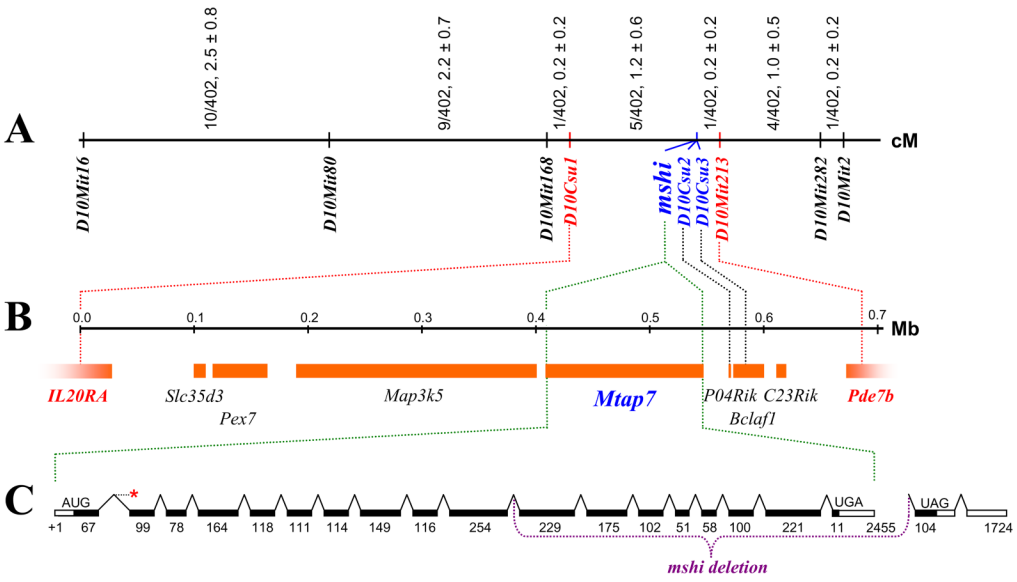

Fig. 1.

Genetic and physical mapping of the mouse *mshi* locus. (*A*) Genetic map based on a 402-member (C57BL/6J × BALB/cByJ-*mshi*/J)F_1 × BALB/c-*mshi*/J backcross, typed for 6 regional microsatellite DNA markers (Rule et al. 1999), and 3 single-nucleotide polymorphisms. The number of recombinants out of 402 total backcross mice, and the percent recombination (± 1 standard error) are shown in each interval. *D10Csu1* and *D10Mit213* are aliases for *IL20RA* and *Pde7b*, and define the maximal location of *mshi*. (*B*) The known genes in the critical region between *D10Csu1* and *D10Mit213* (Ensembl Mouse 2008) are drawn on a 0.1 Mb scale. Three of these candidates, *Mtap7*, *P04Rik*, and *Bclaf1* were investigated further (see text). *D10Csu2* and *D10Csu3* are aliases for *Bclaf1* and *P04Rik*, respectively. (*C*) Genomic structure of the *Mtap7* gene. Solid black boxes indicate the 18 exons that comprise *Mtap7*, an asterisk indicates the location of the $Mtap7^{k.o.}$ *βgal/neo* insertion in Intron 1–2 (Komada et al. 2000), and a dotted bracket indicates the extent of the 13,080 bp deletion that defines the mutant *mshi* allele. The number below each exon is the number of basepairs each contains. In the mutant, Exon 10 is spliced to two downstream cryptic exons, designated Exon 11M and 12M. The number at the right end of the final exon in the wild and mutant transcript is the length of the mRNA in nucleotides.

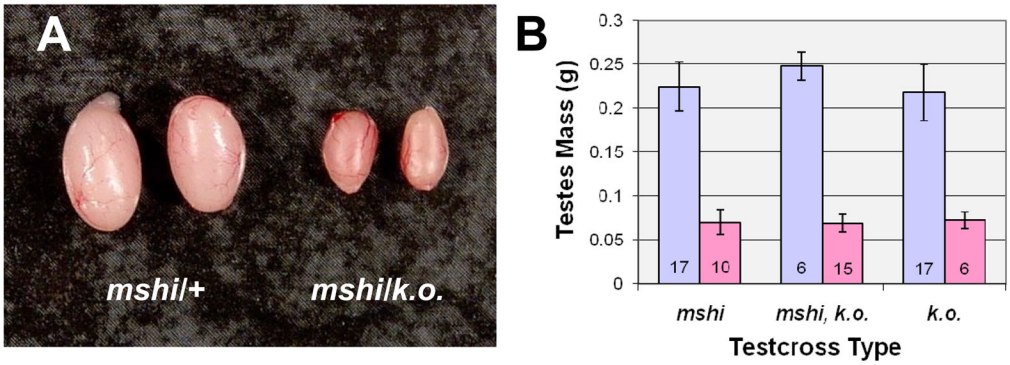

Fig. 2.

Testis size displayed by three-month-old males with various *Mtap7* genotypes. (*A*) Testes testes from heterozygous control (*mshi*/+) and mutant (*mshi*/*Mtap7*$^{k.o.}$) mice. (*B*) Mass of testes from 3-month old heterozygous controls and homozygous mutants from 3 different test crosses: *mshi*/*mshi* × *mshi*/+ (left), *Mtap7*$^{k.o.}$/*Mtap7*$^{k.o.}$ × *Mtap7*$^{k.o.}$/+ (center), and *mshi*/*mshi* × *Mtap7*$^{k.o.}$/+ (right). The average (combined) testicular mass is shown, ±1 standard error. The *n* number in each category is shown at the base of each bar.

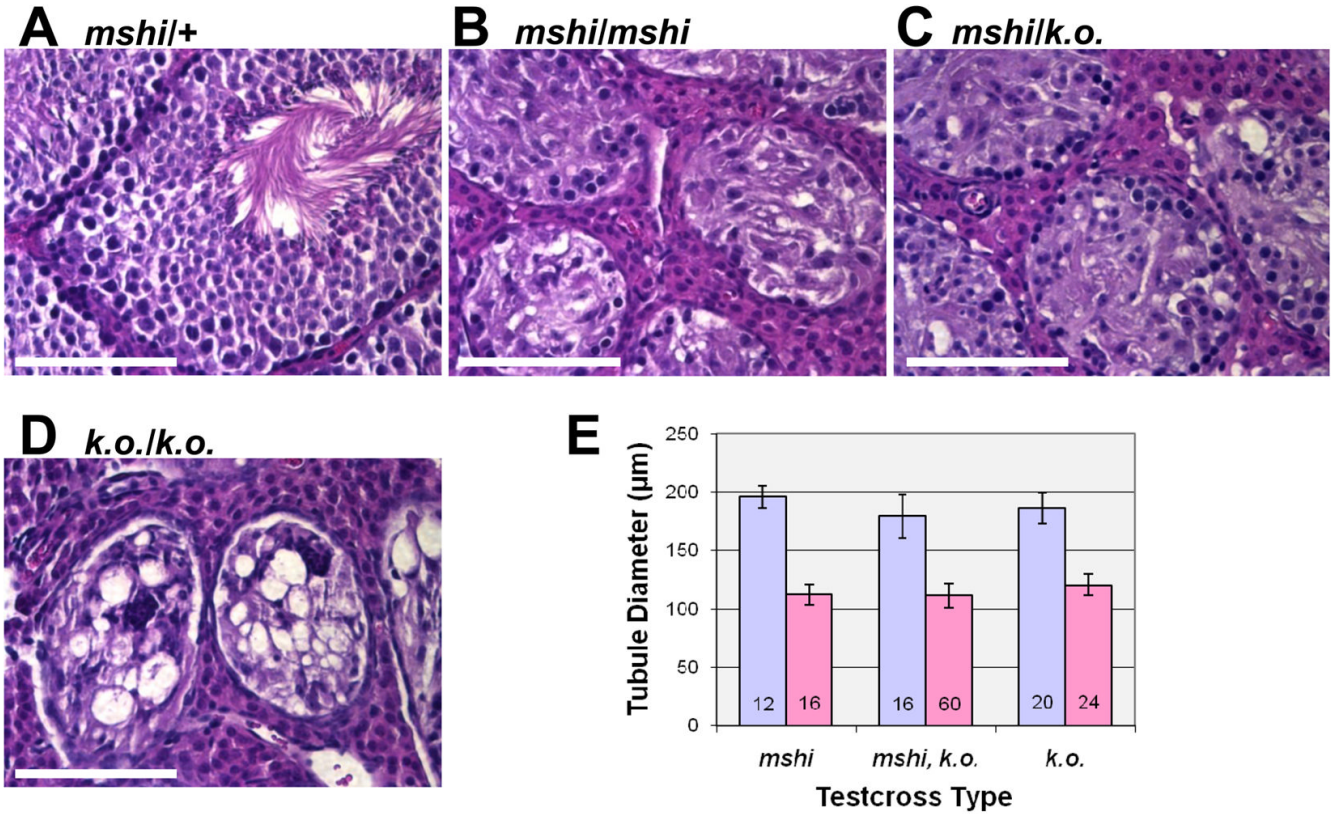

Fig. 3.

Hematoxylin and eosin stained cross sections of testicular tubules of three-month-old heterozygous control (*mshi*/+, *A*), and mutant (*mshi*/*mshi*, *B; mshi*/*Mtap7*$^{k.o.}$, *C*; and *Mtap7*$^{k.o.}$/*Mtap7*$^{k.o.}$, *D*) mice. White bars at the lower left measure 100 μm. (*E*) Diameter of testicular tubules from heterozygous controls and homozygous mutants from 3 different test crosses: *mshi*/*mshi* × *mshi*/+ (left), *Mtap7*$^{k.o.}$/*Mtap7*$^{k.o.}$ × *Mtap7*$^{k.o.}$/+ (center), and *mshi*/*mshi* × *Mtap7*$^{k.o.}$/+ (right). The average tubule diameter is shown, ±1 standard error. The number of individual testicular cross sections examined (*n*) in each category is shown at the base of each bar; four different tubules from each testicular cross section were measured.

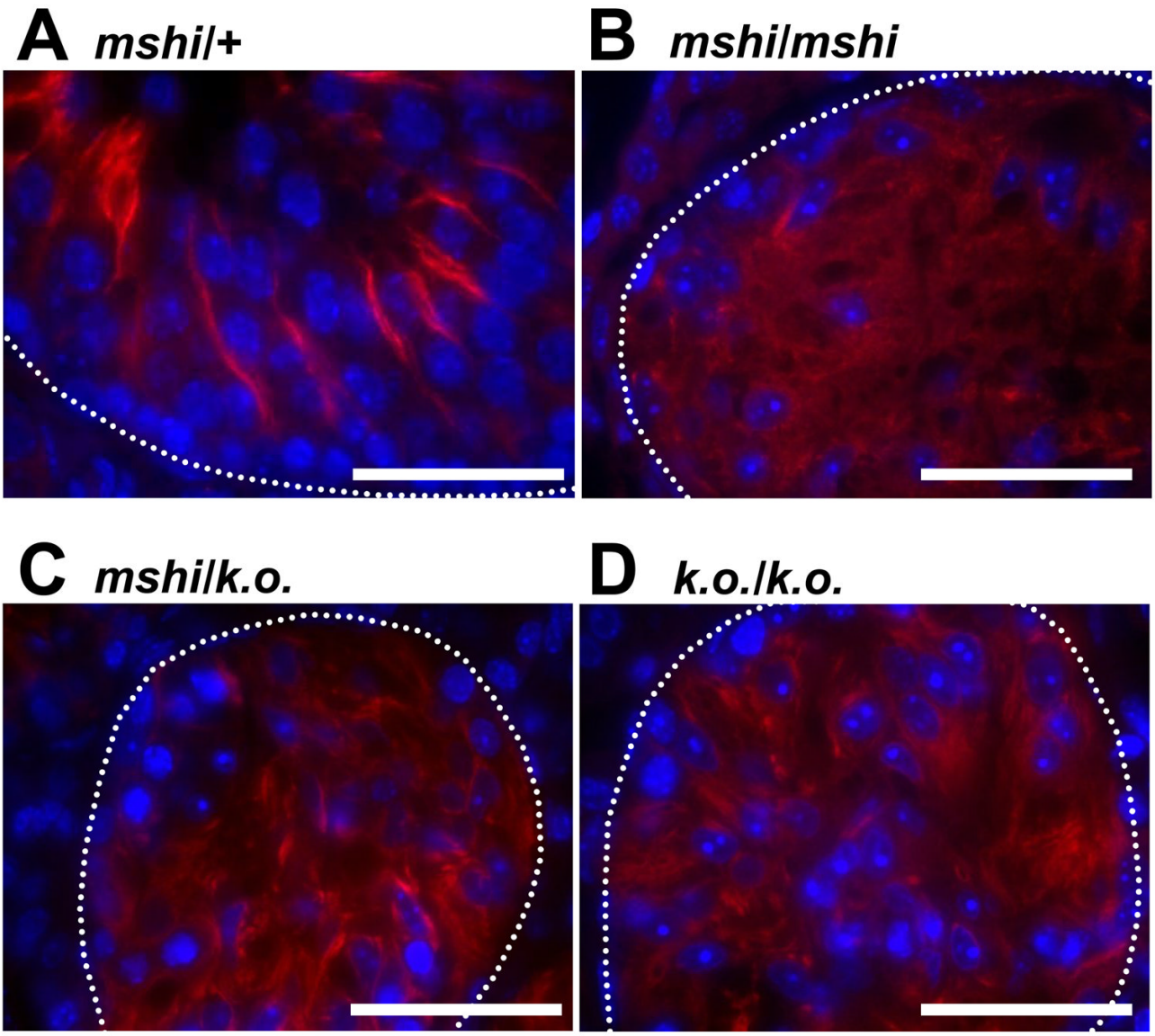

Fig. 4.

Morphology of microtubules in three-month-old heterozygous control (*mshi*/+, *A*), and mutant (*mshi*/*mshi*, *B; mshi*/*Mtap7*$^{k.o.}$, *C*; and *Mtap7*$^{k.o.}$/*Mtap7*$^{k.o.}$, *D*) mice. Testicular sections were stained with anti-β-tubulin antibody (red), nuclei were costained with Hoechst's reagent (blue). Basement membranes of the seminiferous tubules are indicated by broken lines. White bars at the lower right measure 50 μm.

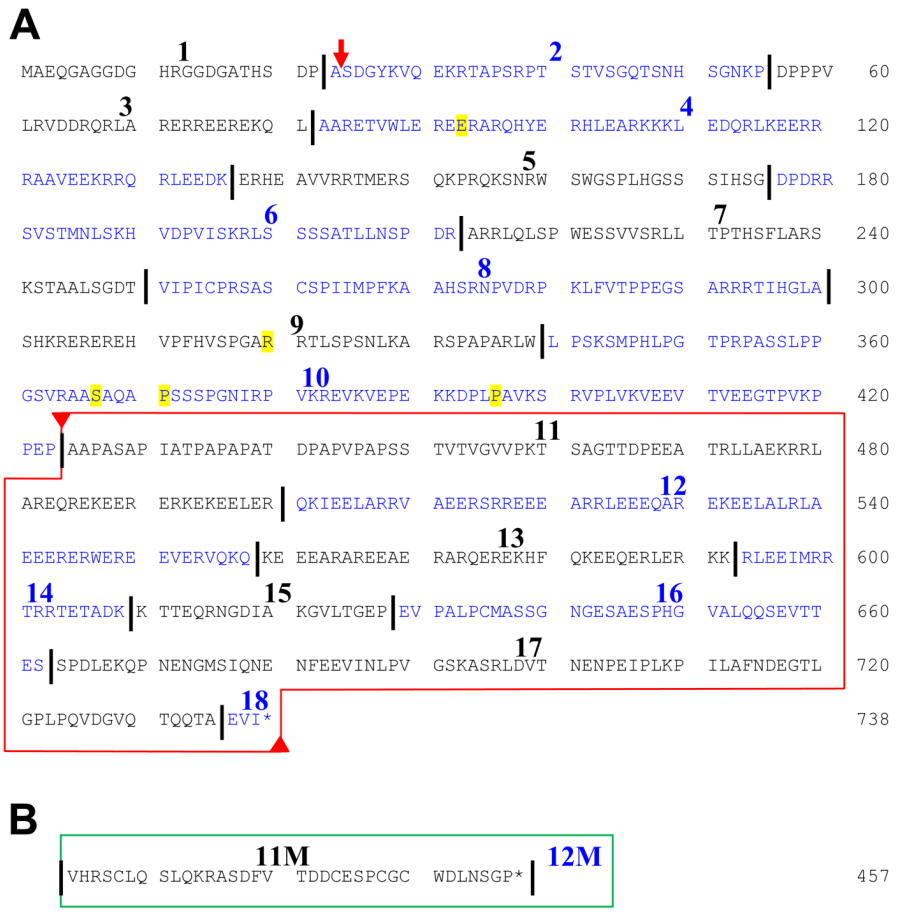

Fig. 5.

Sequence analysis of *Mtap7*alleles. The predicted amino acid sequence for the wild type (*A*) and *mshi* mutant allele of *Mtap7* are shown (*B*). The wild type sequence was based on the C57BL/6J and the BALB/cByJ inbred strains of mice. Black bars indicate the exon boundaries; the red arrow indicates the position of the *βgal/neo* insertion in $Mtap7^{k.o.}$ (Komada et al. 2000); single-nucleotide differences between C57BL/6J and BALB/cByJ (in Exons 4, and 9, and 10) are highlighted in yellow (although all of these third-positions variants are silent, see Fig. S1). The section of the wild-type protein that is boxed in red is deleted in the mutant *mshi* allele, and is replaced with the green-boxed sequence in part *B* due to splicing of Exon 10 to two exons, designated 11M and 12M, that are downstream of the deletion breakpoint. The DNA sequence that defines the *mshi* deletion is shown in Fig. S2. The DNA sequence of mutant Exons 11M and 12M are shown in Fig. S3.